

On the Performance of HAPS-assisted Hybrid RF-FSO Multicast Communication Systems

Olfa Ben Yahia, Eylem Erdogan, *Senior Member, IEEE*, Gunes Karabulut Kurt, *Senior Member, IEEE*

Abstract—Multicast routing is considered a promising approach for real-time applications to address the massive data traffic demands. In this work, we study the outage probability of a multicast downlink communication network for non-terrestrial communication systems. More precisely, we propose two practical use-cases. In the former model, we propose a high altitude platform station (HAPS) aided mixed radio frequency (RF)/free-space optical (FSO)/RF communication scheme where a terrestrial ground station intends to communicate with a cluster of nodes through two stratospheric HAPS systems. In the latter model, we assume that the line of sight (LOS) connectivity is inaccessible between the two HAPS systems due to high attenuation caused by large propagation distances. Thereby, we propose a low Earth orbit (LEO) satellite-aided mixed RF/FSO/FSO/RF communication. For the proposed scenarios, outage probability expressions are derived and validated with Monte Carlo (MC) simulations under different conditions.

Index Terms—High altitude platform station, multicast transmission, outage probability, stratospheric attenuation.

I. INTRODUCTION

Given the fast growth of real-time applications, high demands for higher throughput, lower latency, and better quality of service, new standardization become essential. In sixth generation (6G) networks, it is envisioned that data transmission will be conducted over vertical heterogeneous networks, known as VHetNets, which is composed of three layers including space network, aerial network, and terrestrial network [1]. Low Earth orbit (LEO) satellites, which are the components of space networks, can provide low round trip delay and a high data rate. In this regard, they become a potent enabler for real-time traffic such as voice and video for global coverage, especially in remote areas, where wired communication is challenging or cannot be employed.

High altitude platform station (HAPS) systems which are positioned in the stratosphere around 20 km, can combine the characteristics of the terrestrial network (low cost and latency) and satellites (wide coverage area), draw the attention of both academia and the industrial communities [2]. HAPS systems are quasi-stationary aerial vehicles that suffer less from atmospheric turbulence as they are positioned above the cloud formations [3]. However, HAPS systems are prone to stratospheric attenuation, which can be caused by sulfuric acid

ingredients due to volcanic activity, gases, and polar clouds [4].

To successfully fulfill the high data rate requirements, free-space optical (FSO) communication links can be an important enabler for the non-terrestrial networks. FSO communication ensures high data rate transmission with a low probability of interception [5], [6]. However, FSO communication is subject to atmospheric turbulence and it is weather-dependent. Also, the performance of FSO links can be degraded by scintillation, beam spreading, and beam wander causing significant diffraction effects. More specifically, for the uplink communication, beam wander needs to be considered as it produces a large long-term spot size and produces a significant pointing error that causes serious fluctuations in the transmitted signal. However, in the downlink communication, the effect of beam wander can be neglected, whereas pointing error is still an important drawback as satellites are in motion. In optical communications, aperture averaging, in which a larger aperture diameter is used at the receiver, can be adopted to mitigate the adverse effects of pointing errors and turbulence-induced fading [7]. Furthermore, optical beam is limited to masking effects over large distances and the line-of-sight (LOS) connectivity can not be established between the satellites and the multicast users due to shadowing and obstacles. Thus, in satellite communication (SatCom), cooperative relaying in which a HAPS system can be used as an intermediate relay node, can be considered as an effective solution to mitigate the channel impairments [8], [9].

With the increase of the proliferation of streaming media, video conference, IP-TV, and many other applications of broadcast communication, it is expected that the spectral efficiency of wireless communications can be enhanced by serving a group of users simultaneously [10]. Therefore, multicasting is well suitable for these services as it exploits the resources of the network efficiently. According to the international telecommunication union (ITU) recommendations, a multicast group is defined as a set of nodes that have specified their intention to receive packets on a particular multicast group address [11]. Several research works have been conducted to investigate multicasting protocols. In [12], the authors optimize the transmission data rates of the base station and thus maximizes the multicast capacity considering an average outage constraint. The authors in [13] introduce a new low-computational radio resource management scheme based on a low complexity greedy algorithm for multicast grouping. To achieve a better reliability and spectral utilization, the authors in [14] propose the integration of non-orthogonal multiple access (NOMA) within multicast communication.

O. Ben Yahia and G. Karabulut Kurt are with the Department of Electronics and Communication Engineering, Istanbul Technical University, Istanbul, Turkey, (e-mails: {yahiao17, gkurt}@itu.edu.tr).

E. Erdogan is with the Department of Electrical and Electronics Engineering, Istanbul Medeniyet University, Istanbul, Turkey, (e-mail: eylem.erdogan@medeniyet.edu.tr).

G. Karabulut Kurt is also with the Department of Electrical Engineering, Polytechnique Montréal, Montréal, QC, Canada (e-mail: gunes.kurt@polymtl.ca).

Furthermore, cooperative relaying in multicast achieves great diversity gain, which is affected by the number of relays [15]. In [16], outage probability (OP), as well as diversity gain expressions, are derived for cooperative multicast systems with the best relay selection. In [17], the HAPS node is integrated into Universal Mobile Telecommunications Systems (UMTS) leading to enhanced system efficiency in terms of resource capacity, coverage area, and the number of simultaneously active users. Considering geostationary Earth orbit (GEO) to HAPS architecture, the authors propose a reliable multicast protocol, where the HAPS node ensures the local transmission [18]. Different from the current literature, in this paper, we propose two new use-cases for multicast services. By addressing the above challenges, this paper makes the following contributions:

- In this work, two use-cases have been proposed for multicast downlink communication. In the first one, we consider a ground transmitter communicating with a multicast group through the use of two intermediate HAPS systems. In the second use-case, the communication is conducted through two HAPS systems connected with a LEO satellite.
- For the optical SatCom, we investigate the effect of beam wander-induced pointing error for the uplink, the effect of aperture averaging technique and pointing error for the downlink, and the effect of shadowing severity for RF communication.
- We derive closed-form outage probability expressions for both scenarios by considering stratospheric attenuation, stratospheric turbulence induced-fading for FSO communication, and shadowing and fading for RF communication.

The rest of this paper is organized as follows. In Section II the signals and system model are presented. The expressions of outage probability are derived in Section III. Numerical results are provided and analyzed in Section IV. Finally, the conclusion is drawn in Section V.

II. SIGNALS AND SYSTEM MODEL

In this section, we illustrate the proposed system model of downlink communication for multicast protocol. As shown in Fig. 1, we consider two use-cases. In both cases, we assume the presence of a ground transmitter G that intends to send its information to a set of N ground destinations $D = \{D_1, D_2, \dots, D_N\}$ registered under the same multicast address and distributed randomly at hundreds of kilometers far from each other. More precisely, in the first use-case (s_1), the transmission is completed through two HAPS nodes \mathcal{H}_1 and \mathcal{H}_2 by using optical communication as perfect LOS is established between them. In the second use-case (s_2), the LOS connectivity can not be formed between \mathcal{H}_1 and \mathcal{H}_2 due to large distance, non-static stratospheric winds, or stratospheric attenuation. Thereby, a LEO satellite-aided optical cooperation is created over three network layers. In particular, G transmits its message to the multicast group in four-time slots over \mathcal{H}_1 , the LEO satellite S , and \mathcal{H}_2 , all working based on decode and forward (DF) relaying protocol. In both scenarios, the uplink from G to \mathcal{H}_1 and the downlink from \mathcal{H}_2 to D are

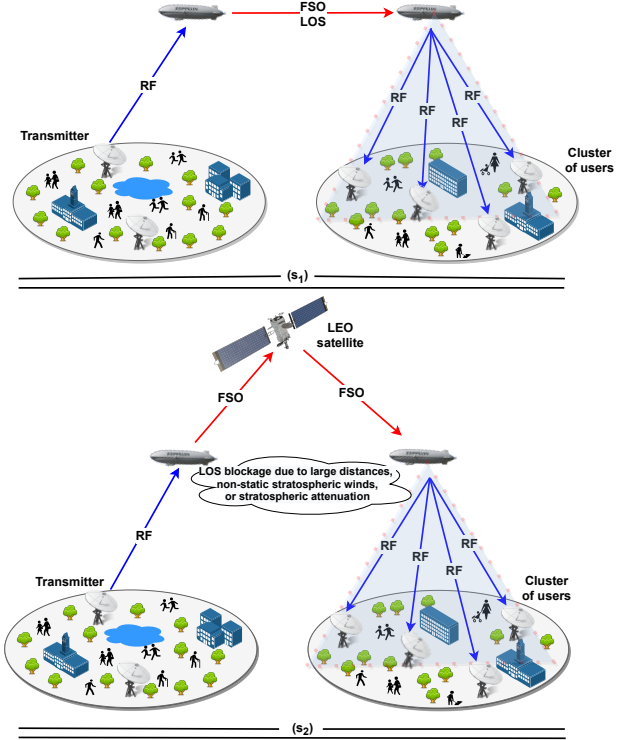


Fig. 1: Illustration of the two models. s_1) HAPS-aided mixed RF/FSO/RF and s_2) Satellite-aided mixed RF/FSO/FSO/RF communication with multicast clustering.

conducted through RF links, that experience the shadowed-Rician fading. The FSO links on the other hand follow the exponentiated Weibull (EW) fading. Furthermore, we assume that \mathcal{H}_2 is deploying a multi-beam antenna, which makes it able to project multiple spot beams within its potential footprint.

A. HAPS-aided Mixed RF/FSO/RF Communication

1) Ground-to-HAPS Communication

In the first hop, we assume that RF communication is used due to the destructive effects of aerosols, gases, and atmospheric conditions that highly affect the performance of FSO communication. Thereby, in the first phase, the received signal at \mathcal{H}_1 can be given as

$$y_{\mathcal{H}_1} = \sqrt{P_G \mathcal{F}_{\mathcal{H}_1}} h_{G, \mathcal{H}_1} x_G + n_{\mathcal{H}_1}, \quad (1)$$

where P_G denotes the transmit power of G , $\mathcal{F}_{\mathcal{H}_1}$ indicates the path loss, h_{G, \mathcal{H}_1} is the channel coefficient between G and \mathcal{H}_1 , x_G represents the transmitted symbol with $\mathbb{E}\{|x_G|^2\} = 1$, with $\mathbb{E}\{\cdot\}$ is the statistical expectation operator, and $n_{\mathcal{H}_1}$ is the zero-mean complex Gaussian noise at \mathcal{H}_1 with noise power spectral density (PSD) N_0 . Based on (1), the instantaneous SNR at \mathcal{H}_1 can be written as

$$\gamma_{G, \mathcal{H}_1} = \frac{P_G \mathcal{F}_{\mathcal{H}_1}}{N_0} |h_{G, \mathcal{H}_1}|^2 = \bar{\gamma}_{G, \mathcal{H}_1} |h_{G, \mathcal{H}_1}|^2, \quad (2)$$

where $\bar{\gamma}_{G, \mathcal{H}_1} = \frac{P_G \mathcal{F}_{\mathcal{H}_1}}{N_0}$ is the average SNR of the RF link. Furthermore, the path loss of the RF communication can be

given as [19]

$$\mathcal{F}_{\mathcal{H}_1}[dB] = G_T + G_R - L_F - L_R - L_A, \quad (3)$$

where G_T , G_R denote the transmit and the receiver antenna gains respectively, L_F indicates the free space path loss given as $L_F = 92.45 + 20 \log f_r + 20 \log L_{G,\mathcal{H}_1}$, f_r represents the frequency in GHz, L_{G,\mathcal{H}_1} represents the propagation distance from G to \mathcal{H}_1 , L_R indicates the attenuation due to rain in dB/km, and L_A is the gaseous atmosphere loss.

In this work, we consider shadowed-Rician distribution. The probability density function (PDF) of the envelope of the channel gain $|h_{G,\mathcal{H}_1}|$ can be written as [19]

$$f_{|h_{G,\mathcal{H}_1}|^2}(h) = \left(\frac{2b_{\mathcal{H}_1}m_{\mathcal{H}_1}}{2b_{\mathcal{H}_1}m_{\mathcal{H}_1} + \Omega_{\mathcal{H}_1}} \right)^{m_{\mathcal{H}_1}} \frac{h}{2b_{\mathcal{H}_1}} \exp\left(\frac{-h^2}{2b_{\mathcal{H}_1}}\right) \times {}_1F_1\left(m_{\mathcal{H}_1}; 1; \frac{\Omega_{\mathcal{H}_1}h^2}{2b_{\mathcal{H}_1}(2b_{\mathcal{H}_1}m_{\mathcal{H}_1} + \Omega_{\mathcal{H}_1})}\right), \quad (4)$$

where $m_{\mathcal{H}_1}$ denoting the Nakagami- m fading severity parameter of the corresponding channel, $2b_{\mathcal{H}_1}$ is the average power of the non-LOS (NLOS) components, $\Omega_{\mathcal{H}_1}$ represents the average power of LOS component, and ${}_1F_1(\cdot; \cdot; \cdot)$ denotes the confluent hypergeometric function which is given in [20, eqn. 07.20.03.0108.01]. Therefore, after a few manipulations, we derive the PDF of the instantaneous SNR γ_{G,\mathcal{H}_1} as [21]

$$f_{\gamma_{G,\mathcal{H}_1}}(\gamma) = \sum_{j=0}^{m_{\mathcal{H}_1}-1} \frac{\vartheta_{\mathcal{H}_1}(1-m_{\mathcal{H}_1})_j \cdot (-\delta_{\mathcal{H}_1})^j}{\bar{\gamma}_{G,\mathcal{H}_1}^{j+1} \cdot (j!)^2} \times \gamma^j \exp(-\psi_{\mathcal{H}_1}\gamma), \quad (5)$$

where $\vartheta_{G,\mathcal{H}_1} = \frac{1}{2b_{\mathcal{H}_1}} \left(\frac{2b_{\mathcal{H}_1}m_{\mathcal{H}_1}}{2b_{\mathcal{H}_1}m_{\mathcal{H}_1} + \Omega_{\mathcal{H}_1}} \right)^{m_{\mathcal{H}_1}}$, $\psi_{\mathcal{H}_1} = \frac{\varsigma_{\mathcal{H}_1} - \delta_{G,\mathcal{H}_1}}{\bar{\gamma}_{G,\mathcal{H}_1}}$, $\varsigma_{\mathcal{H}_1} = \frac{1}{2b_{\mathcal{H}_1}}$, $\delta_{\mathcal{H}_1} = \frac{\Omega_{\mathcal{H}_1}}{2b_{\mathcal{H}_1}(2b_{\mathcal{H}_1}m_{\mathcal{H}_1} + \Omega_{\mathcal{H}_1})}$, and $(\cdot)_j$ is the Pochhammer symbol. In this regard, the cumulative distribution function (CDF) of γ_{G,\mathcal{H}_1} is given by

$$F_{\gamma_{G,\mathcal{H}_1}}(\gamma) = 1 - \sum_{l=0}^{m_{\mathcal{H}_1}-1} \sum_{q=0}^l \frac{\vartheta_{\mathcal{H}_1}(1-m_{\mathcal{H}_1})_l \cdot (-\delta_{\mathcal{H}_1})^l}{q!(\psi_{\mathcal{H}_1})^{l-q+1} (\bar{\gamma}_{G,\mathcal{H}_1})^{l+1} l!} \times (\gamma)^q \exp(-\psi_{\mathcal{H}_1}\gamma). \quad (6)$$

2) Inter-HAPS Communication

Herein, we use FSO communication as LOS conditions can be perfectly satisfied due to the quasi-stationary position of HAPS systems. In the second phase of communication, the received signal at \mathcal{H}_2 can be given as [5]

$$y_{\mathcal{H}_2} = \zeta \sqrt{P_{\mathcal{H}_1}} I_{\mathcal{H}_1,\mathcal{H}_2} x_{\mathcal{H}_1} + n_{\mathcal{H}_2}, \quad (7)$$

where ζ indicates the electrical-to-optical conversion coefficient, $P_{\mathcal{H}_1}$ is the average transmitted optical power of \mathcal{H}_1 , $x_{\mathcal{H}_1}$ is the transmitted signal of \mathcal{H}_1 , and $I_{\mathcal{H}_1,\mathcal{H}_2} > 0$ represents the received fading gain (irradiance) between the laser of \mathcal{H}_1 and the photodetector of \mathcal{H}_2 through the optical link. Finally, $n_{\mathcal{H}_2}$ is the zero-mean complex Gaussian noise at \mathcal{H}_2 with noise PSD N_0 . Thus, the instantaneous SNR at \mathcal{H}_2 can be written as

$$\gamma_{\mathcal{H}_1,\mathcal{H}_2} = \frac{\zeta P_{\mathcal{H}_1} I_{\mathcal{H}_1,\mathcal{H}_2}^2}{N_0} = \bar{\gamma}_{\mathcal{H}_1,\mathcal{H}_2} I_{\mathcal{H}_1,\mathcal{H}_2}^2, \quad (8)$$

where $\bar{\gamma}_{\mathcal{H}_1,\mathcal{H}_2}$ indicates the average SNR.

In FSO communication, the channel gain can be considered as a composite optical channel as $I_{\mathcal{H}_1,\mathcal{H}_2} = I_{\mathcal{H}_1,\mathcal{H}_2}^a I_{\mathcal{H}_1,\mathcal{H}_2}^t$ [5], where $I_{\mathcal{H}_1,\mathcal{H}_2}^a$ defines the stratospheric attenuation and $I_{\mathcal{H}_1,\mathcal{H}_2}^t$ models the stratospheric turbulence. The effect of stratospheric turbulence can be modeled by using the EW fading distribution. Thus, the PDF of $I_{\mathcal{H}_1,\mathcal{H}_2}^t$ can be expressed as

$$f_{I_{\mathcal{H}_1,\mathcal{H}_2}^t}(I) = \frac{\alpha_{\mathcal{H}_1,\mathcal{H}_2} \beta_{\mathcal{H}_1,\mathcal{H}_2}}{\eta_{\mathcal{H}_1,\mathcal{H}_2}} \left(\frac{I}{\eta_{\mathcal{H}_1,\mathcal{H}_2}} \right)^{\beta_{\mathcal{H}_1,\mathcal{H}_2} - 1} \times \exp \left[- \left(\frac{I}{\eta_{\mathcal{H}_1,\mathcal{H}_2}} \right)^{\beta_{\mathcal{H}_1,\mathcal{H}_2}} \right] \times \left(1 - \exp \left[- \left(\frac{I}{\eta_{\mathcal{H}_1,\mathcal{H}_2}} \right)^{\beta_{\mathcal{H}_1,\mathcal{H}_2}} \right] \right)^{\alpha_{\mathcal{H}_1,\mathcal{H}_2} - 1}, \quad (9)$$

where $\eta_{\mathcal{H}_1,\mathcal{H}_2}$ is the scale parameter, and $\alpha_{\mathcal{H}_1,\mathcal{H}_2}$, $\beta_{\mathcal{H}_1,\mathcal{H}_2}$ denote the shape parameters which are directly related to the scintillation index. These parameters can be expressed as [22]

$$\alpha_{\mathcal{H}_1,\mathcal{H}_2} = \frac{7.220 \times \sigma_{I_{\mathcal{H}_1,\mathcal{H}_2}}^{2/3}}{\Gamma(2.487 \sigma_{I_{\mathcal{H}_1,\mathcal{H}_2}}^{2/6} - 0.104)},$$

$$\beta_{\mathcal{H}_1,\mathcal{H}_2} = 1.012 \left(\alpha_{\mathcal{H}_1,\mathcal{H}_2} \sigma_{I_{\mathcal{H}_1,\mathcal{H}_2}}^2 \right)^{-13/25} + 0.142,$$

$$\eta_{\mathcal{H}_1,\mathcal{H}_2} = \frac{1}{\alpha_{\mathcal{H}_1,\mathcal{H}_2} \Gamma(1 + 1/\beta_{\mathcal{H}_1,\mathcal{H}_2}) \mathfrak{g}_1(\alpha_{\mathcal{H}_1,\mathcal{H}_2}, \beta_{\mathcal{H}_1,\mathcal{H}_2})}, \quad (10)$$

where $\Gamma(\cdot)$ indicates the Gamma function and $\mathfrak{g}_1(\alpha_{\mathcal{H}_1,\mathcal{H}_2}, \beta_{\mathcal{H}_1,\mathcal{H}_2})$ is the $\alpha_{\mathcal{H}_1,\mathcal{H}_2}$ and $\beta_{\mathcal{H}_1,\mathcal{H}_2}$ dependent constant variable given by [23]

$$\mathfrak{g}_1(\alpha_{\mathcal{H}_1,\mathcal{H}_2}, \beta_{\mathcal{H}_1,\mathcal{H}_2}) = \sum_{k=0}^{\infty} \frac{(-1)^k \Gamma(\alpha_{\mathcal{H}_1,\mathcal{H}_2})}{k!(k+1)^{1+1/\beta_{\mathcal{H}_1,\mathcal{H}_2}} \Gamma(\alpha_{\mathcal{H}_1,\mathcal{H}_2} - k)}, \quad (11)$$

and $\sigma_{I_{\mathcal{H}_1,\mathcal{H}_2}}^2$ is the scintillation index which can be written as [24, Sect. (5)]

$$\sigma_{I_{\mathcal{H}_1,\mathcal{H}_2}}^2 = 1.23 C_n^2 K^{7/6} L_{\mathcal{H}_1,\mathcal{H}_2}^{11/7}. \quad (12)$$

In the above equation, C_n^2 indicates the refractive index structure parameter [24, Sect. (5)], $K = \frac{2\pi}{\lambda}$ is the optical wave number, λ is the optical wavelength, and $L_{\mathcal{H}_1,\mathcal{H}_2}$ represents the propagation distance between \mathcal{H}_1 and \mathcal{H}_2 . According to [25], the communication between two HAPS systems at an altitude of 20 km, is feasible up to 600 km. Herein, it is worth mentioning that the LOS distance might be slightly different from the distance when projecting the HAPS systems on the Earth, due to the curvature nature of the Earth. For inter-HAPS communication, we consider the effect of stratospheric attenuation, which can be defined as the attenuation of the laser beam caused by molecular absorption, scattering by ice crystals, and some other rare phenomenons such as polar clouds, which are connected to the temperature inside the stratosphere, and stratospheric aerosols that depend on the volcanic activity [4]. The stratospheric attenuation can be

modeled based on the Beer-Lambert law as

$$I_{\mathcal{H}_1, \mathcal{H}_2}^a = \exp(-\phi L_{\mathcal{H}_1, \mathcal{H}_2}), \quad (13)$$

where ϕ denotes the stratospheric attenuation coefficient [4].

3) HAPS-to-Ground Communication

In the \mathcal{H}_2 to D multicast communication, the optical signal at \mathcal{H}_2 is converted to electrical signal and then transmitted to D . Therefore, the received signal at the i -th receiver D_i can be expressed as

$$y_{D_i} = \sqrt{P_{\mathcal{H}_2} \mathcal{F}_{D_i}} h_{\mathcal{H}_2, D_i} x_{\mathcal{H}_2} + n_{D_i}, \quad (14)$$

where $P_{\mathcal{H}_2}$ represents the transmit power of \mathcal{H}_2 , \mathcal{F}_{D_i} indicates the path loss, $h_{\mathcal{H}_2, D_i}$ defines the channel information, $x_{\mathcal{H}_2}$ is the transmitted signal from \mathcal{H}_2 , and n_{D_i} is the Gaussian noise with N_0 noise PSD. Accordingly, the instantaneous SNR at the multicast destination can be written as

$$\gamma_{\mathcal{H}_2, D} = \max(\gamma_{\mathcal{H}_2, D_1}, \gamma_{\mathcal{H}_2, D_2}, \dots, \gamma_{\mathcal{H}_2, D_N}). \quad (15)$$

Thus the CDF of $\gamma_{\mathcal{H}_2, D}$ becomes

$$F_{\gamma_{\mathcal{H}_2, D}}(\gamma) = \prod_{i=1}^N \left(1 - \sum_{l=0}^{m_{D_i}-1} \sum_{q=0}^l \frac{\vartheta_{D_i}(1-m_{D_i})_l (-\delta_{D_i})^l}{q!(\psi_{D_i})^{l-q+1} (\bar{\gamma}_{\mathcal{H}_2, D_i})^{l+1} l!} \right) \times (\gamma)^q \exp(-\psi_{D_i} \gamma), \quad (16)$$

Finally, the end-to-end instantaneous SNR at the multicast group D for s_1 can be obtained to be

$$\gamma_0^{s_1} = \min \{ \gamma_{G, \mathcal{H}_1}; \gamma_{\mathcal{H}_1, \mathcal{H}_2}; \gamma_{\mathcal{H}_2, D} \}. \quad (17)$$

B. Satellite-aided mixed RF/FSO/FSO/RF Communication

In this subsection, we present the satellite-aided mixed RF/FSO/FSO/RF communication. The G to \mathcal{H}_1 and \mathcal{H}_2 to D communications were presented in the above section. Thereby, we omit these sections to prevent duplication.

1) HAPS-to-Satellite Communication

In the \mathcal{H}_1 to S communication, the received signal can be expressed very similar to (7) as $y_S = \zeta \sqrt{P_{\mathcal{H}_1}} I_{\mathcal{H}_1, S} x_{\mathcal{H}_1} + n_S$, where $I_{\mathcal{H}_1, S}$ indicates the turbulence induced fading at S . The received SNR at S can be written similar to (8) after changing subscripts $\mathcal{H}_1, \mathcal{H}_2$ with \mathcal{H}_1, S as $\gamma_{\mathcal{H}_1, S} = \frac{\zeta P_{\mathcal{H}_1} I_{\mathcal{H}_1, S}^2}{N_0}$. where the average SNR can be expressed as $\bar{\gamma}_{\mathcal{H}_1, S} = \frac{\zeta P_{\mathcal{H}_1}}{N_0}$. Therefore, the CDF of $\gamma_{\mathcal{H}_1, S}$ can be written as

$$F_{\gamma_{\mathcal{H}_1, S}}(\gamma) = \sum_{\rho=0}^{\infty} \binom{\alpha_{\mathcal{H}_1, S}}{\rho} (-1)^\rho \times \exp \left[-\rho \left(\frac{\gamma}{\eta_{\mathcal{H}_1, S}^2 \bar{\gamma}_{\mathcal{H}_1, S}} \right)^{\frac{\beta_{\mathcal{H}_1, S}}{2}} \right], \quad (18)$$

where $\alpha_{\mathcal{H}_1, S}$, $\beta_{\mathcal{H}_1, S}$, and $\eta_{\mathcal{H}_1, S}$ are the shape parameters and the scale parameter between \mathcal{H}_1 and S respectively as defined in (10). In uplink communication, beam wander-induced pointing error effects should be taken into consideration. Thereby,

the scintillation index for the uplink communication can be written as [24, Sect. (12)]

$$\sigma_{I_{\mathcal{H}_1, S}}^2 = 5.95(H_S - H_{\mathcal{H}_1})^2 \sec^2(\xi_{\mathcal{H}_1, S}) \left(\frac{2W_0}{r_0} \right)^{5/3} \left(\frac{\alpha_{pe}}{W} \right)^2 + \exp \left[\frac{0.49\sigma_{Bu}^2}{(1 + (1.11 + \Theta)\sigma_{Bu}^{12/5})^{7/6}} + \frac{0.51\sigma_{Bu}^2}{(1 + 0.69\sigma_{Bu}^{12/5})^{5/6}} \right] - 1, \quad (19)$$

where H_S denotes the altitude of S , $H_{\mathcal{H}_1}$ is the altitude of \mathcal{H}_1 above the ground level, $\xi_{\mathcal{H}_1, S}$ is the zenith angle between the \mathcal{H}_1 and S , W_0 indicates the beam radius at \mathcal{H}_1 , and r_0 is the Fried's parameter given as

$$r_0 = \left[0.42 \sec(\xi_{\mathcal{H}_1, S}) K^2 \int_{H_{\mathcal{H}_1}}^{H_S} C_n^2(h) dh \right]^{-3/5}. \quad (20)$$

In uplink communication, $C_n^2(h)$ is written as

$$C_n^2(h) = 0.00594 \left(\frac{u_S}{27} \right)^2 (10^{-5} h)^{10} \exp \left(-\frac{h}{1000} \right) + 2.7 \times 10^{-16} \exp \left(-\frac{h}{1500} \right) + C_0 \exp \left(-\frac{h}{100} \right), \quad (21)$$

where $u_S = \sqrt{v_S^2 + 30.69v_S + 348.91}$ is the root-mean-square (RMS) of the wind speed, v_S is the wind speed in m/s, C_0 is the nominal value of C_n^2 at the receiver. Generally, C_n^2 varies from $10^{-12} \text{ m}^{-2/3}$ for the strong turbulence to $10^{-17} \text{ m}^{-2/3}$ for the weak turbulence [26]. In addition, $\alpha_{pe} = \frac{\sigma_{pe}}{L_{\mathcal{H}_1, S}}$ describes the beam wander-induced pointing error, $L_{\mathcal{H}_1, S}$ denotes the propagation distance from \mathcal{H}_1 to S , and σ_{pe}^2 is the beam wander-induced pointing errors variance given as

$$\sigma_{pe}^2 = 0.54(H_S - H_{\mathcal{H}_1}) \sec^2(\xi_{\mathcal{H}_1, S}) \left(\frac{\lambda}{2W_0} \right)^2 \left(\frac{2W_0}{r_0} \right)^{5/3} \times \left[1 - \left(\frac{C_r^2 W_0^2 / r_0^2}{1 + C_r^2 W_0^2 / r_0^2} \right)^{1/6} \right], \quad (22)$$

where C_r is a scaling constant, which is assumed as π for $\lambda = 1550 \text{ nm}$. Furthermore, W indicates the beam size at the receiver, which is given as $W = w_0 \sqrt{\Theta_0^2 + \Lambda_0^2}$, where Λ_0 and Θ_0 denote the beam parameters at the transmitter, which can be expressed as $\Theta_0 = 1 - L_{\mathcal{H}_1, S} / F_0$ and $\Lambda_0 = \frac{2L_{\mathcal{H}_1, S}}{K(w_0)^2}$. F_0 is the phase front radius of curvature at the transmitter and $\Theta = \frac{\Theta_0}{\Theta_0^2 + \Lambda_0^2}$. Finally, σ_{Bu}^2 can be expressed as

$$\sigma_{Bu}^2 = 8.7\mu_{3u} K^{7/6} (H_S - H_{\mathcal{H}_1})^{5/6} \sec^{11/6}(\xi_{\mathcal{H}_1, S}), \quad (23)$$

where μ_{3u} is given as

$$\mu_{3u} = \Re \int_{H_{\mathcal{H}_1}}^{H_S} C_n^2(h) [i\varepsilon(1-\varepsilon)]^{5/6} dh, \quad (24)$$

and ε is the normalized distance variable given as $\varepsilon = 1 - (h - H_{\mathcal{H}_1}) / (H_S - H_{\mathcal{H}_1})$ for the uplink communication.

2) Satellite-to-HAPS Communication

The received signal at \mathcal{H}_2 from the S can be similarly expressed as in (7) by just replacing the subscripts as $y_{\mathcal{H}_2} =$

$\zeta\sqrt{P_S}I_{S,\mathcal{H}_2}x_S+n_{\mathcal{H}_2}$, whereas $I_{S,\mathcal{H}_2} = I_{S,\mathcal{H}_2}^a I_{S,\mathcal{H}_2}^t I_{S,\mathcal{H}_2}^p$ with I_{S,\mathcal{H}_2}^p defines the pointing error component caused by the fast rotation of the LEO satellite. Thereafter, the instantaneous SNR can be written as given in (8) by changing the subscripts $\mathcal{H}_1, \mathcal{H}_2$ with S, \mathcal{H}_2 . $\alpha_{S,\mathcal{H}_2}, \beta_{S,\mathcal{H}_2}, \eta_{S,\mathcal{H}_2}$ can be derived using the same equations given in the previous section, and the scintillation index for S to \mathcal{H}_2 can be written as [24, Sect. (12)]. Furthermore, pointing error is considered as one of the major impairments of FSO communication as it involves the displacement of the communicating nodes. In the presence of non-zero boresight pointing errors, the PDF of I_{S,\mathcal{H}_2}^p can be expressed as [27]

$$f_{I_{S,\mathcal{H}_2}^p}(I^p) = \frac{g^2 \exp\left(\frac{-s^2}{2\sigma_s^2}\right)}{A_0^2} (I^p)^{g^2-1} I_0\left(\frac{s}{\sigma_s^2} \sqrt{\frac{-w_{eq}^2 \ln \frac{I^p}{A_0}}{2}}\right), \quad (25)$$

where $g = w_{eq}/2\sigma_s$ represents the ratio between the equivalent beamwidth w_{eq} and the jitter standard deviation σ_s , which indicates the severity of the pointing error effects. Furthermore, $s = 0$ since we are considering zero boresight error, $A_0 = [\text{erf}(v)]^2$ denotes the gathered optical power for zero difference between the optical spot center and the detector center, where $v = \sqrt{\pi/2}a/w_z$ is the ratio of the aperture radius a and the beamwidth w_z at distance z with $w_z = \theta z$ with θ is the transmit divergence angle [27]. Finally, $I_0(x)$ defines the modified Bessel function of the first kind with order zero. In the presence of pointing error, the CDF of γ_{S,\mathcal{H}_2} becomes [7]

$$F_{\gamma_{S,\mathcal{H}_2}}(\gamma) = \frac{\alpha_{S,\mathcal{H}_2} g^2}{\beta_{S,\mathcal{H}_2}} \left(\frac{1}{\eta_{S,\mathcal{H}_2} A_0 \sqrt{\gamma}} \right)^{g^2} \times \sum_{i=0}^{\infty} T_2(i) G_{2,3}^{2,1} \left(T_3(i) \left| \begin{matrix} 1 - T_1, 1 \\ 0, 1 - T_1, -T_1 \end{matrix} \right. \right). \quad (26)$$

In (26), $G_{p,q}^{m,n}(x | a_1, \dots, a_p; b_1, \dots, b_q)$ denotes the Meijer G-function [20, eqn. 07.34.02.0001.01], $T_1 = g^2/\beta_{S,\mathcal{H}_2}$, $T_2(i) = (-1)^i \Gamma(\alpha_{S,\mathcal{H}_2}) / [i! \Gamma(\alpha_{S,\mathcal{H}_2} - i) (1+i)^{1-T_1}]$, and $T_3(i) = (1+i) \left(\frac{1}{\eta_{S,\mathcal{H}_2} A_0 \sqrt{\gamma}} \right)^{\beta_{S,\mathcal{H}_2}}$. In the satellite to HAPS communication, we apply the aperture averaging technique as it can reduce signal fluctuations. Therefore, the aperture size-dependent scintillation index can be expressed as [24, Sect. (12)]

$$\sigma_{I_{S,\mathcal{H}_2}}^2 = 8.7k^{7/6} (H_S - H_{\mathcal{H}_2})^{5/6} \text{sec}^{11/6} (\xi_{S,\mathcal{H}_2}) \times \Re \left\{ \int_{H_{\mathcal{H}_2}}^{H_S} C_n^2(h) \left[\left(\frac{kD_G^2}{16L_{S,\mathcal{H}_2}} + i \frac{h - H_{\mathcal{H}_2}}{H_S - H_{\mathcal{H}_2}} \right)^{5/6} - \left(\frac{kD_G^2}{16L_{S,\mathcal{H}_2}} \right)^{5/6} \right] dh \right\}. \quad (27)$$

For s_2 , the end-to-end instantaneous SNR at the multicast destination D can then be obtained as

$$\gamma_0^{s_2} = \min \{ \gamma_{G,\mathcal{H}_1}; \gamma_{\mathcal{H}_1,S}; \gamma_{S,\mathcal{H}_2}; \gamma_{\mathcal{H}_2,D} \}, \quad (28)$$

where $\gamma_{\mathcal{H}_2,D}$ is the instantaneous SNR at the destination which can be written very similar to (2).

III. OUTAGE PROBABILITY

The outage probability (OP) can be described as the probability that the instantaneous SNR γ_0 falls below a predefined outage threshold γ_{out} and it can be written as

$$P_{out} = \Pr[\gamma_0 \leq \gamma_{out}]. \quad (29)$$

More precisely, the OP can be derived from the CDF of the end-to-end SNR γ_0 as $P_{out} = F_{\gamma_0}(\gamma_{out})$. Furthermore, in the case of multi-hop communication, the OP is the probability that the transmitted message is not decoded correctly by at least one of the users at the end of the communication. Thus, the OP expression for s_1 can be given as [5]

$$P_{out}^{s_1}(\gamma_{out}) = 1 - \left[(1 - F_{\gamma_{G,\mathcal{H}_1}}(\gamma_{out})) (1 - F_{\gamma_{\mathcal{H}_1,\mathcal{H}_2}}(\gamma_{out})) \times (1 - F_{\gamma_{\mathcal{H}_2,D}}(\gamma_{out})) \right], \quad (30)$$

where $F_{\gamma_{\mathcal{H}_1,\mathcal{H}_2}}(\gamma)$ indicates the CDF of $\gamma_{\mathcal{H}_1,\mathcal{H}_2}$. For s_2 , the OP can be written as

$$P_{out}^{s_2}(\gamma_{out}) = 1 - \left[(1 - F_{\gamma_{G,\mathcal{H}_1}}(\gamma_{out})) (1 - F_{\gamma_{\mathcal{H}_1,S}}(\gamma_{out})) \times (1 - F_{\gamma_{S,\mathcal{H}_2}}(\gamma_{out})) (1 - F_{\gamma_{\mathcal{H}_2,D}}(\gamma_{out})) \right]. \quad (31)$$

The final expressions of the OP for both scenarios are given at the top of the next page as (32) and (33).

IV. NUMERICAL RESULTS AND DISCUSSIONS

In this section, we investigate the performance of our proposed setup based on the theoretical derivations developed in the previous sections. We first verify the derived expressions with Monte Carlo (MC) simulations. For RF communication, we consider different shadowing severity levels: frequent heavy shadowing ($m = 1.0, b = 0.063, \Omega = 8.94 \times 10^{-4}$), average shadowing ($m = 10, b = 0.126, \Omega = 0.835$), and infrequent light shadowing ($m = 19, b = 0.158, \Omega = 1.29$) [21]. For the first use-case s_1 , we assume $C_n^2 = 10^{-18} \text{ m}^{-2/3}$ and different propagation distances between the two HAPS systems. For the second use-case s_2 , the LEO satellite is located at 500 km of altitude, both HAPS systems are at altitude of 18 km. Furthermore, the beam radius at \mathcal{H}_1 is set to $W_0 = 2 \text{ cm}$, $C_0 = 10^{-18} \text{ m}^{-2/3}$, $\xi_{\mathcal{H}_1,S} = \xi_{S,\mathcal{H}_2} = 70^\circ$, and $u_S = u_{\mathcal{H}_2} = 65 \text{ m/s}$. For stratospheric attenuation, we consider the case of molecular absorption at the HAPS node, which is $\phi = 10^{-5}$. For all figures, the outage threshold is set to $\gamma_{out} = 7 \text{ dB}$.

Fig. 2 illustrates the OP as a function of average SNR per hop for a different number of multicast users when the source experiences the average shadowing and the destination experiences the frequent heavy shadowing level. As we can see from the figure, the theoretical results are in good agreement with the MC simulations. In addition, it is obvious that increasing the propagation distance between the HAPS systems deteriorates the overall performance as the scintillation index $\sigma_{I_{\mathcal{H}_1,\mathcal{H}_2}}^2$ increases with the distance from 0.6925 to 1.7667, which means that the turbulence induced-fading can severely

$$\begin{aligned}
P_{out}^{s_1}(\gamma_{out}) = & 1 - \left[\left(1 - \left(1 - \sum_{l=0}^{m_{\mathcal{H}_1}-1} \sum_{q=0}^l \frac{\vartheta_{\mathcal{H}_1}(1-m_{\mathcal{H}_1})_l \cdot (-\delta_{\mathcal{H}_1})^l}{q!(\psi_{\mathcal{H}_1})^{l-q+1}(\bar{\gamma}_{G,\mathcal{H}_1})^{l+1}l!} (\gamma_{out})^q \exp(-\psi_{\mathcal{H}_1}(\gamma_{out})) \right) \right) \times \left(1 - \sum_{\rho=0}^{\infty} \binom{\alpha_{\mathcal{H}_1,\mathcal{H}_2}}{\rho} \right) \right. \\
& \times (-1)^\rho \exp \left[-\rho \left(\frac{\gamma_{out}}{(\eta_{\mathcal{H}_1,\mathcal{H}_2} I^l)^2 \bar{\gamma}_{\mathcal{H}_1,\mathcal{H}_2}} \right)^{\frac{\beta_{\mathcal{H}_1,\mathcal{H}_2}}{2}} \right] \left. \times \left(1 - \prod_{i=1}^N \left(1 - \sum_{l=0}^{m_{D_i}-1} \sum_{q=0}^l \frac{\vartheta_{D_i}(1-m_{D_i})_l \cdot (-\delta_{D_i})^l}{q!(\psi_{D_i})^{l-q+1}(\bar{\gamma}_{\mathcal{H}_2,D_i})^{l+1}l!} (\gamma_{out})^q \exp(-\psi_{D_i}(\gamma_{out})) \right) \right) \right] \\
& \times (\gamma_{out})^q \exp(-\psi_{D_i}(\gamma_{out})) \left. \right], \tag{32}
\end{aligned}$$

$$\begin{aligned}
P_{out}^{s_2}(\gamma_{out}) = & 1 - \left[\left(1 - \left(1 - \sum_{l=0}^{m_{\mathcal{H}_1}-1} \sum_{q=0}^l \frac{\vartheta_{\mathcal{H}_1}(1-m_{\mathcal{H}_1})_l \cdot (-\delta_{\mathcal{H}_1})^l}{q!(\psi_{\mathcal{H}_1})^{l-q+1}(\bar{\gamma}_{G,\mathcal{H}_1})^{l+1}l!} (\gamma_{out})^q \exp(-\psi_{\mathcal{H}_1}(\gamma_{out})) \right) \right) \times \left(1 - \sum_{\rho=0}^{\infty} \binom{\alpha_{\mathcal{H}_1,\mathcal{H}_2}}{\rho} \right) \right. \\
& \times (-1)^\rho \exp \left[-\rho \left(\frac{\gamma_{out}}{\eta_{\mathcal{H}_1,S}^2 \bar{\gamma}_{\mathcal{H}_1,S}} \right)^{\frac{\beta_{\mathcal{H}_1,S}}{2}} \right] \left. \times \left(1 - \sum_{\rho=0}^{\infty} \binom{\alpha_{S,\mathcal{H}_2}}{\rho} (-1)^\rho \exp \left[-\rho \left(\frac{\gamma_{out}}{(\eta_{S,\mathcal{H}_2} I^l)^2 \bar{\gamma}_{S,\mathcal{H}_2}} \right)^{\frac{\beta_{S,\mathcal{H}_2}}{2}} \right] \right) \right] \\
& \times \left(1 - \prod_{i=1}^N \left(1 - \sum_{l=0}^{m_{D_i}-1} \sum_{q=0}^l \frac{\vartheta_{D_i}(1-m_{D_i})_l \cdot (-\delta_{D_i})^l}{q!(\psi_{D_i})^{l-q+1}(\bar{\gamma}_{\mathcal{H}_2,D_i})^{l+1}l!} (\gamma_{out})^q \exp(-\psi_{D_i}(\gamma_{out})) \right) \right) \left. \right]. \tag{33}
\end{aligned}$$

affect the communication quality. Furthermore, as expected, serving more users at the same time enhances the performance as the number of receivers increases.

In Fig. 3, we evaluate the OP performance of the HAPS-aided scenario for different shadowing levels. Precisely, we consider a propagation distance of 100 km between the HAPS systems and a cluster of 10 ground users. Moreover, we assume that the transmitter and the receivers experience the same shadowing level. It is clear from the figure that decreasing the shadowing level improves the overall outage performance.

Fig. 4 evaluates the OP of the second scenario s_2 . For the HAPS to satellite (\mathcal{H}_1, S) and satellite to HAPS communication (S, \mathcal{H}_2), we consider the same zenith angle and same wind

speed. The simulation results showed that the scintillation index is the same for uplink and downlink communications even when considering the presence of beam wander-induced pointing error and this is due to the fact that the HAPS node is located above the clouds' level and it is less sensitive to channel distortion. Furthermore, from this figure, we can observe that the results agree well with MC simulations validating our theoretical expressions. Also, we can see that the OP significantly enhances by increasing the number of downlink receivers. Finally, we observe that, increasing the Nakagami-m severity parameter boosts the OP performance.

In Fig. 5, we examine the outage performance of s_2 by considering the impact of pointing errors in the downlink

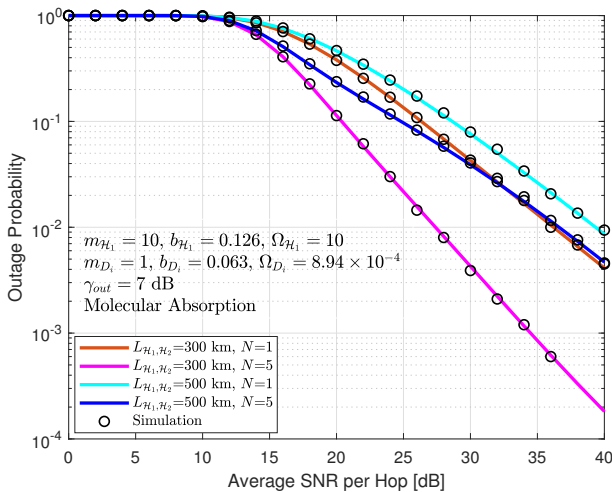


Fig. 2: Outage probability performance of s_1 for different number of multicast users and HAPS distances $L_{\mathcal{H}_1,\mathcal{H}_2}$.

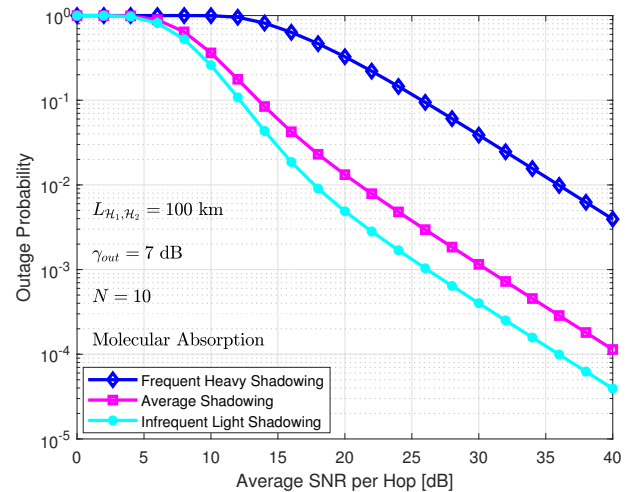


Fig. 3: Outage probability performance of s_1 for various shadowing levels.

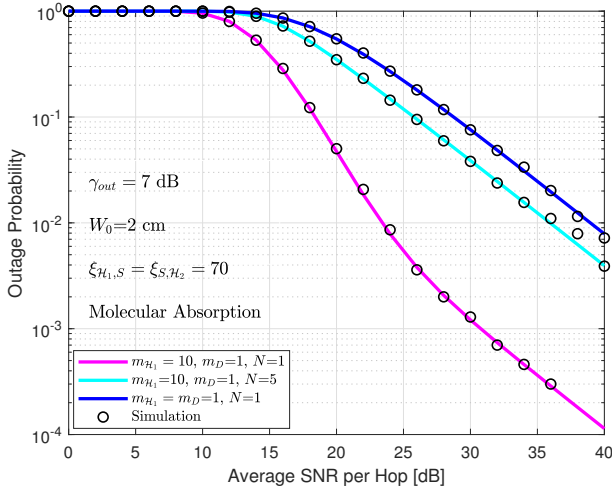


Fig. 4: Outage probability performance of s_2 for different shadowing levels and various number of multicast users.

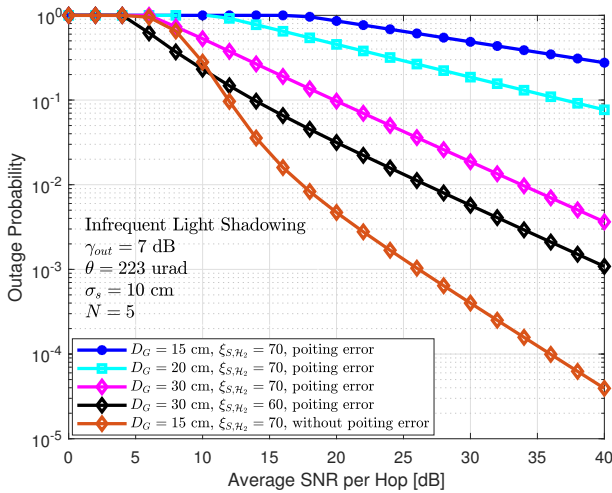


Fig. 5: Outage probability performance of s_2 for various aperture sizes in the presence of pointing error at \mathcal{H}_2 .

FSO communication for different aperture sizes. The beam divergence angle is set to $\theta = 225$ urad [28] and the jitter standard deviation is taken as $\sigma_s = 10$ cm. As expected, the presence of pointing errors deteriorates the communication and this is due to the misalignment between the satellite and the HAPS \mathcal{H}_2 . As illustrated in the figure, increasing the aperture size improves the overall performance as it increases the amount of gathered information. Furthermore, choosing lower values of the zenith angle can yield better performance of the proposed scheme.

Fig. 6 compares the OP performance of the proposed scenarios. For the first scenario, we consider two different propagation distances between \mathcal{H}_1 and \mathcal{H}_2 . For the second scenario, we assume $\xi_{\mathcal{H}_1,S} = \xi_{S,\mathcal{H}_2} = 70^\circ$ and $u_S = u_{\mathcal{H}_2} = 65$ m/s, which results in 2.6486×10^3 km of separation between the two HAPS systems. For both scenarios, we consider five multicast users and that all RF communication experience

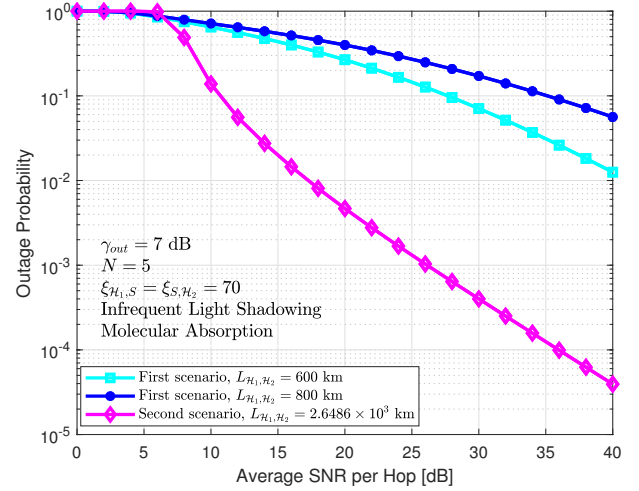


Fig. 6: Comparison of s_1 and s_2 in terms of outage probability.

infrequent light shadowing. It is inferred from the figure that for larger distances between the communicating users, the second scenario is more practical as it performs better even in windy weather and high zenith angles. As expected, at higher propagation distances, the overall performance of the first use-case decreases.

Finally, some major design guidelines can be summarized as follows:

- We observe from the results that the effect of beam wander-induced pointing error from HAPS to satellite is almost negligible. Thus, deploying a HAPS node as a relay between the ground station and the LEO satellite significantly improves the uplink performance.
- The results have shown that multicast services can increase the diversity gain and achieves a better outage performance.
- The simulations have shown that the use of a LEO satellite can be a promising solution for inter-HAPS communication when HAPS systems are deployed far from each other.
- The results have shown that the presence of pointing errors in downlink FSO communication deteriorates the overall performance. However, decreasing the zenith angle or increasing the aperture size of the receiver lens can mitigate the impact of pointing errors as they decrease the impact of stratospheric turbulence.

V. CONCLUSION

In this paper, we proposed two different use-cases for multicast applications namely HAPS-aided mixed RF/FSO/RF and satellite-aided mixed RF/FSO/FSO/RF schemes. For the proposed setups, outage probability expressions are derived in closed-form by considering shadowed-Rician fading for RF links and EW fading for FSO communication. The derived expressions are validated with MC simulations. For the proposed models, we investigated the impact of beam wander, pointing errors, zenith angle, and aperture averaging technique for FSO communications and the impact of shadowing level for RF communication. From the results, we observed that the use

of HAPS as an intermediate node in uplink SatCom alleviates the impact of beam wander-induced pointing error. In addition, the results showed that for larger distances, the satellite-aided mixed RF/FSO/FSO/RF scenario performed better. Finally, the aperture averaging technique can be adopted to minimize the effect of atmospheric turbulence and improve communication in the presence of misalignment errors.

REFERENCES

- [1] G. Karabulut Kurt, M. G. Khoshkholgh, S. Alfattani, A. Ibrahim, T. S. J. Darwish, M. S. Alam, H. Yanikomeroglu, and A. Yongacoglu, "A vision and framework for the high altitude platform station (HAPS) networks of the future," *IEEE Communications Surveys Tutorials*, vol. 23, no. 2, pp. 729–779, 2021.
- [2] S. Gharbi, N. Zangar, and N. Aitsaadi, "Overview: High altitude platform network for disaster and crises application," in *Int. Conf. on Info. and Commun. Technol. for Disaster Management (ICT-DM)*, 2019.
- [3] F. Fidler, M. Knapek, J. Horwath, and W. R. Leeb, "Optical communications for high-altitude platforms," *IEEE Journal of Selected Topics in Quantum Electronics*, vol. 16, no. 5, pp. 1058–1070, 2010.
- [4] D. Giggenbach, R. Purvinskis, M. Werner, and M. Holzbock, "Stratospheric optical inter-platform links for high altitude platforms," in *Int. Commun. Satellite Sys. Conf. and Exhibit*, 2002, p. 1910.
- [5] E. T. Michailidis, N. Nomikos, P. Bithas, D. Vouyioukas, and A. G. Kanatas, "Outage probability of triple-hop mixed RF/FSO/RF stratospheric communication systems," in *IEEE Int. Conf. on Adv. in Satellite and Space Commun. (SPACOMM)*, 2018, pp. 1–6.
- [6] E. Erdogan, "On the performance of cognitive underlay RF/FSO communication systems with limited feedback," *Optics Communications*, vol. 444, pp. 87–92, 2019.
- [7] Y. Wang, P. Wang, X. Liu, and T. Cao, "On the performance of dual-hop mixed RF/FSO wireless communication system in urban area over aggregated exponentiated weibull fading channels with pointing errors," *Optics Communications*, vol. 410, pp. 609–616, 2018.
- [8] K. Guo, M. Lin, B. Zhang, J.-B. Wang, Y. Wu, W.-P. Zhu, and J. Cheng, "Performance analysis of hybrid satellite-terrestrial cooperative networks with relay selection," *IEEE Trans. on Veh. Technol.*, vol. 69, no. 8, pp. 9053–9067, 2020.
- [9] O. B. Yahia, E. Erdogan, G. K. Kurt, I. Altunbas, and H. Yanikomeroglu, "HAPS selection for hybrid RF/FSO satellite networks," *arXiv preprint arXiv:2107.12638*, 2021.
- [10] Z. Wang, Q. Liu, M. Li, and W. Kellerer, "Energy efficient analog beamformer design for mmwave multicast transmission," *IEEE Trans. on Green Commun. and Netw.*, vol. 3, no. 2, pp. 552–564, 2019.
- [11] ITU-R, "Multicast IP performance parameters." International Telecommunication Union, Recommendation Y.1544, 2003.
- [12] H. Wang, X. Chu, and H. Xiang, "Capacity maximization and transmission rates optimization for relay assisted wireless multicast," *IEEE Commun. Letters*, vol. 16, no. 10, pp. 1592–1595, 2012.
- [13] G. Araniti, A. Orsino, J. Cosmas, A. Molinaro, and A. Iera, "A low computational-cost subgrouping multicast scheme for emerging 5G-satellite networks," in *IEEE International Symposium on Broadband Multimedia Systems and Broadcasting (BMSB)*, 2016, pp. 1–6.
- [14] L. Yang, J. Chen, Q. Ni, J. Shi, and X. Xue, "NOMA-enabled cooperative unicast-multicast: Design and outage analysis," *IEEE Transactions on Wireless Communications*, vol. 16, no. 12, pp. 7870–7889, 2017.
- [15] Hui Tian, Youyun Xu, Wei Xie, Jiang Yu, and Liubin Song, "Outage probability analysis of opportunistic cooperative multicast based on coded cooperation," in *Int. Conf. on Commun. Technol.*, 2010, pp. 1035–1038.
- [16] I. Lee, H. Lee, and H. Choi, "Exact outage probability of relay selection in decode-and-forward based cooperative multicast systems," *IEEE Communications Letters*, vol. 17, no. 3, pp. 483–486, 2013.
- [17] G. Araniti, A. Iera, and A. Molinaro, "The effect of multicast user number and distribution on the performance of RRM policies in terrestrial-HAP MBMS systems," in *IEEE Global Telecommunications Conference*, 2007, pp. 5037–5041.
- [18] I. Alocci, M. Berioli, N. Celandroni, G. Giambene, and S. Karapantazis, "Proposal of a reliable multicast protocol in a HAP-satellite architecture," in *Vehicular Technology Conference*, 2007, pp. 1380–1384.
- [19] S. R. S. Sharma, N. Vishwakarma, and A. Madhukumar, "HAPS-based relaying for integrated space-air-ground networks with hybrid FSO/RF communication: A performance analysis," *IEEE Trans. on Aerospace and Electronic Systems*, pp. 1–1, 2021.
- [20] The Wolfram functions site. [Online]. Available: <http://www.wolfram.com>
- [21] Y. Ai, A. Mathur, M. Cheffena, M. R. Bhatnagar, and H. Lei, "Physical layer security of hybrid satellite-FSO cooperative systems," *IEEE Photon. J.*, vol. 11, no. 1, pp. 1–14, 2019.
- [22] R. Barrios Porras, *Exponentiated Weibull fading channel model in free-space optical communications under atmospheric turbulence*. Ph.D. dissertation, Dept. Signal Theory Commun., Univ. Politècnica de Catalunya (UPC), Barcelona, Spain, May 2013.
- [23] E. Erdogan, I. Altunbas, G. K. Kurt, M. Bellemare, G. Lamontagne, and H. Yanikomeroglu, "Site diversity in downlink optical satellite networks through ground station selection," *IEEE Access*, vol. 9, pp. 31 179–31 190, 2021.
- [24] L. C. Andrews and R. L. Phillips, *Laser Beam Propagation through Random Media (SPIE Press Monograph)*, 2005.
- [25] D. F. Fidler, *Optical Communications from High-Altitude Platforms*. Ph.D. dissertation, Vienna University of Technology, Vienna, Austria, September 2007.
- [26] Z. Ghassemlooy, W. Popoola, and S. Rajbhandari, *Optical Wireless Communications: System and Channel Modelling with Matlab*. CRC Press, 2019.
- [27] F. Yang, J. Cheng, and T. A. Tsiftsis, "Free-space optical communication with nonzero boresight pointing errors," *IEEE Trans. on Commun.*, vol. 62, no. 2, pp. 713–725, 2014.
- [28] D. R. Kolev and M. Toyoshima, "Satellite-to-ground optical communications using small optical transponder (SOTA)-received-power fluctuations," *Optics Express*, vol. 25, no. 23, pp. 28 319–28 329, 2017.